Geophysical Research Letters

RESEARCH LETTER
10.1029/2025GL115023

Thermohaline Preconditioning for Sea Ice Formation in the Beaufort Sea

O. J. Houndegnonto[1,2], I. G. Fenty[1], S. Fournier[1], M. Steele[3], M. J. Zahn[1,3], and P. Gaube[4]

[1]Jet Propulsion Laboratory, California Institute of Technology, Pasadena, CA, USA, [2]International Chair in Mathematical Physics and Applications (ICMPA-UNESCO Chair), Université d'Abomey-Calavi, Abomey-Calavi, Benin, [3]Applied Physics Laboratory, Polar Science Center, University of Washington, Seattle, WA, USA, [4]Air-Sea Interaction and Remote Sensing Department, Applied Physics Laboratory, University of Washington, Seattle, WA, USA

Key Points:

- Near-surface salt-stratified layers promote early sea ice formation
- A salt-stratified layer promotes heat retention beneath the surface mixed layer
- Once sea ice starts to form, heat above the pycnocline acts to reduce the growth rate

Supporting Information:

Supporting Information may be found in the online version of this article.

Correspondence to:

O. J. Houndegnonto,
Odilon.Houndegnonto@gmail.com

Citation:

Houndegnonto, O. J., Fenty, I. G., Fournier, S., Steele, M., Zahn, M. J., & Gaube, P. (2025). Thermohaline preconditioning for sea ice formation in the Beaufort Sea. *Geophysical Research Letters*, *52*, e2025GL115023. https://doi.org/10.1029/2025GL115023

Received 21 FEB 2025
Accepted 13 AUG 2025

Author Contributions:

Conceptualization: O. J. Houndegnonto, I. G. Fenty
Formal analysis: O. J. Houndegnonto
Funding acquisition: I. G. Fenty, S. Fournier
Investigation: O. J. Houndegnonto
Methodology: O. J. Houndegnonto, I. G. Fenty
Project administration: I. G. Fenty, S. Fournier
Supervision: I. G. Fenty, S. Fournier, M. Steele
Validation: O. J. Houndegnonto
Writing – original draft: O. J. Houndegnonto
Writing – review & editing: I. G. Fenty, S. Fournier, M. Steele, M. J. Zahn, P. Gaube

Abstract The influence of ocean stratification and heat content on the timing of sea ice formation and its subsequent growth remains an open question. Here we investigate the thermohaline conditions prior to fall sea ice formation as well as the roles of stratification and heat content on sea ice growth rates through the analysis of in situ observations and numerical simulations from a one-dimensional ocean-ice-column model. We find that the simulated time series of sea ice concentration are highly correlated with observations. We identify two clusters of sea ice concentration growth rate, which we name Early Slow and Late-Fast. We find that cold, shallow mixed layers promote early sea ice freeze-up. Salinity stratification within the upper pycnocline slows the release of heat into the deepening mixed layer, leading to slower ice growth. However, where salinity stratification above the upper pycnocline is absent, sea ice growth occurs later and, once started, progresses faster.

Plain Language Summary Arctic sea ice is dramatically decreasing, leading to a transient increase in the surface freshwater content of the Beaufort Sea. Sea ice advance during the autumn occurs about a month later than it did just 40 years ago, whereas summer ice melt occurs earlier. However, the role of salinity layering in these changes is still not well understood. In this study, we used a one-dimensional computer model and ocean measurements to examine how seawater salinity layering and ocean heat influence the timing of sea ice formation and its subsequent growth. We found that timing is determined by how much heat is in the upper ocean at the start of freezing. The speed of sea ice growth is then influenced by salinity layering when there is heat at depths below the surface.

1. Introduction

Arctic sea ice cover plays a key role in maintaining the Earth energy balance (Miyawaki et al., 2023; Zhong et al., 2022), leading the Arctic Ocean to be one of the most sensitive areas to global climate change (Francis et al., 2017; Rantanen et al., 2022; Yamanouchi & Takata, 2020). Arctic sea ice is drastically declining with the loss of multiyear sea ice from the western Arctic, notably the Beaufort Sea, while the relative proportion of first-year ice is increasing (Notz & Community, 2020; Schweiger et al., 2021; Wang & Overland, 2015). Consequently, longer duration and more persistent open water and an increase in low surface salinity anomalies from summer ice melt have been observed in the Beaufort Sea, increasing near-surface thermohaline stratification (Toole et al., 2010; Zhang et al., 2023).

Freshwater input from summer ice melt in the Arctic Ocean induces strong salinity stratification, which inhibits vertical mixing and thus the efficiency of surface ventilation of stored subsurface heat as well as the exchange of carbon and oxygen (Li et al., 2020). Subsurface heat storage may also affect the timing of sea ice formation. Previous studies have reported that autumn ice advance now occurs later (by about a month relative to ∼40 *years* ago), while summer ice retreat occurs earlier (Thomson et al., 2022). This change in the timing of sea ice retreat and advance influences Arctic marine ecosystems, human activities that depend on them (e.g., fisheries). However, the role of salinity stratification in sea ice advance and retreat is still not well understood. Understanding how upper ocean salinity influences the timing and growth of sea ice is critical to better predict the impacts of the changing Arctic cryosphere (Ravindran et al., 2021).

The present work aims to understand how upper pycnocline salinity stratification and ocean heat modulate the timing and growth rate of initial sea ice growth in the weeks and months following the September minimum

through the analysis of observations collected during the SASSIE (Salinity and Stratification at Sea Ice Edge, see Drushka et al., 2024) project in the Beaufort Sea and numerical one-dimensional ocean-ice column model simulations. To the best of our knowledge, this is the first study to investigate thermohaline preconditioning for sea ice formation based on 1D ocean simulations during the fall-winter sea ice advance period in the Beaufort Sea. The study is organized as follows: data and methods are described in Section 2, the major results are presented in Section 3 and Section 4 is dedicated to discussion and conclusions.

2. Data and Methods

2.1. Model Configurations and Consistency Evaluation

We use the MIT General Circulation Model (MITgcm) in a one-dimensional ocean-ice column configuration (0-layer thermodynamic ice model, see Text S1 in Supporting Information S1) to investigate how ocean temperature, salinity, and density stratification influence the timing and rate of initial sea ice growth. The model simulates the time evolution of vertical profiles of temperature and salinity, seawater freezing, and the thickening and expansion of sea ice due to atmosphere surface forcing. Vertical ocean mixing is parameterized with the K-profile parameterization of Large et al. (1994). Horizontal advection is not implemented. The model has 70 vertical 1 m layers, with grid centers from 0.5 to 65.5 m depth. Sea ice concentration (SIC) is defined as the fraction per unit area of ocean surface covered by sea ice due to purely thermodynamic processes. The MITgcm "seaice" package parameterizes sea ice thermodynamics based on Hibler (1979). Model simulations are performed with 1 h time steps, from which daily average outputs are saved over approximately 5 months (from 09 Sep 2022 to 31 Jan 2023). The evaluation of the model consistency demonstrates that the mean SIC time series from both model and observations over the simulation period are well correlated ($r = 0.99$) with a Root Mean Square Deviation (RMSD) of 0.07 (See Text S2 and Figure S1 in Supporting Information S1).

2.2. Ocean Model Initial Conditions, Atmospheric Forcing and Observations

The underway CTD (uCTD) salinity (S) and temperature (T) profiles from the SASSIE field campaign (Schmidgall, 2023) are used as the ocean initial conditions (during 09–29 Sept., 2022). In situ T/S profiles were interpolated from 0.1 dbar onto the model's 1 m vertically spaced grid, and converted to potential temperature and absolute salinity (SA, g/kg), respectively using TEOS-10 packages (IOC et al., 2010). Only T/S profiles with first values no deeper than 1 m and with complete measurements in the upper 70 m are considered in our analysis.

For atmospheric forcing, we used 2 m air temperature and specific humidity, and 10 m vector winds, downward longwave and shortwave radiative flux, and precipitation from the MERRA-2 reanalysis (Gelaro et al., 2017; GMAO, 2015a). Bias-corrected precipitation data are taken from M2T1NXFLX (Gelaro et al., 2017; GMAO, 2015b). Downward radiative fluxes are taken from M2T1NXRAD (Gelaro et al., 2017; GMAO, 2015c). MERRA-2 atmospheric fields are provided hourly on a 0.5°× 0.625° latitude-longitude grid from which we form daily mean fields to force the model. The model computes the net heat and freshwater fluxes, including evaporation. Model simulations begin at the time of the uCTD cast and run until 31 Jan. 2023.

For the model SIC relevance analysis, we use the daily 10 km SIC product from OSI SAF EUMETSAT (hereafter AMSR-2), based on the OSI SAF Ice Concentration Algorithm (SAF, 2017). Sea ice motion data are collected from the Polar Pathfinder Daily 25 km EASE-Grid Sea Ice Motion Vectors, Version 4 product (hereafter NSIDC-0116 and used in Supporting Information S1, Tschudi et al. (2019)).

2.3. Stratification Analysis

We classify the upper water column into two adjacent vertical layers whose interface depth changes with time: the mixed layer (ML) and the upper pycnocline layer (UPL) (see Figure 1e). The thickness of the ML (the mixed layer depth, MLD) is defined as the distance between the ocean surface and the depth at which the vertical density gradient increases by 0.03 kg/m^3 relative to the near-surface density at 2.5 m depth (de Boyer Montégut et al., 2004; Sérazin et al., 2023). The UPL is defined as the layer between the base of the ML and the pycnocline depth (PD). The PD−the depth of the top of the pycnocline, is defined as the depth at which ML deepening practically ceases and falls to small value such that $\frac{\partial MLD}{\partial t} \approx 0.0625$ m/day. We find that the ML deepening over fall approaches the top of the pycnocline (equivalent to winter MLD, Cole & Roemer, 2024) when SIC reaches

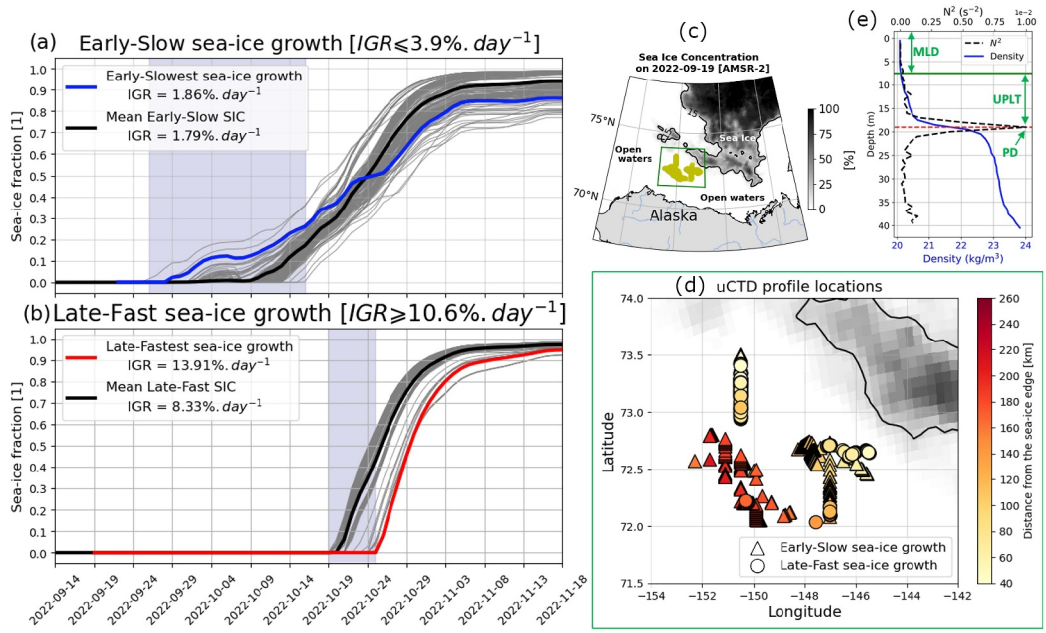

Figure 1. Time series of SIC for (a) Early Slow sea ice growth (No. = 200 time series) and (b) Late-Fast sea ice growth (No. = 200 time series) from the model output. The thick solid black curve (in a, b) is the mean SIC, blue curve (in a) is the time series of the earliest-slowest sea ice growth while the thick solid red curve (in b) is the latest-fastest sea ice growth. (c) SIC map in the Beaufort Sea from AMSR-2 on 19-09-2022 (with the colorbar on panel (c) indicating the SIC). Black solid contour line represents the sea ice edge and yellow dots represent the locations of uCTD casts. (d) Zoom of (c) with uCTD cast locations. The triangle sign ("Δ") and the circle sign ("◯") indicate the locations for Early Slow and Late-Fast sea ice growth profiles, respectively, in the Beaufort Sea. The color-shaded with the colorbar on panel (d) indicate the distance to sea ice edge at the time of uCTD cast. (e) Vertical decomposition of the water column: density profile (solid blue curve) and square of the buoyancy frequency (N^2) profile (dashed black curve). The horizontal green line indicates the surface mixed layer depth (MLD) and the horizontal dashed red line indicates the upper pycnocline layer thickness (UPLT).

80%–95%. The UPL thickness (UPLT) is defined as the distance between the base of the ML and the PD. Once the ML reaches the PD, UPLT is zero.

The timing of sea ice formation and its subsequent growth rate are both influenced by upper ocean thermohaline stratification, as measured by $N^2(z) = -\frac{g}{\rho_0}\frac{d\rho}{dz}$ (i.e., squared vertical buoyancy frequency), which is here decomposed into S and T contributions as:

$$N^2(z) \approx N_S^2(z) + N_T^2(z) \tag{1}$$

where $N_S^2(z) = -g\beta(z)\frac{\partial S}{\partial z}$ *and* $N_T^2(z) = g\alpha(z)\frac{\partial T}{\partial z}$. g is the gravitational acceleration taken as 9.81 m^{2}s^{-1}, α and β are salinity contraction and thermal expansion coefficients, respectively, and z is the depth.

2.4. Thermohaline Flux Analysis

The ocean heat content (OHC) relative to freezing is expressed as follows:

$$OHC = \int_{-h}^{0} c_p(z)\,\rho(z)\left[T(z) - T_{fr}\right]dz \tag{2}$$

where ρ is water density, c_p is the heat capacity estimated with the TEOS-10 package (IOC et al., 2010), $T_{fr} = -1.8$°C is the sea water freezing temperature and h is the targeted depth: MLD or PD.

During sea ice growth, the ML is ventilated by eroding the pycnocline through downward salt rejection and upward heat flux when there is heat below the ML. Sensible heat within the UPL (also referred to here as Thermal

Barrier: TB) suppresses sea ice growth. By the end of the upper pycnocline layer erosion, the initial salt deficit (hereafter SD) created by ice melt is compensated through salt fluxes driving salinity changes (Martinson, 1990). The variation of both TB and SD is tied to the sea ice growth rate. In this study, TB (in m) and SD (in m) are quantified based on the Martinson and Iannuzzi (1998) method as follows:

$$TB = \frac{\rho_w . c_{p_w}}{\rho_i L_i} \int_{z_c}^{0} \left[T(z) - T_{fr} \right] dz \tag{3}$$

$$\mathrm{SD} = \frac{1}{\sigma} \int_{z_c}^{0} \left[S(z) - S_{z_c} \right] dz \tag{4}$$

where $\rho_w = 1027\ \mathrm{kg/m^3}$, $\rho_i = 910\ \mathrm{kg/m^3}$, $c_{p_w} = 4.186$ J/g.°C, and $L_i = 334$ J/g which are the density of seawater, density of sea ice, specific heat of seawater, and latent heat of fusion of sea ice respectively. $\sigma = 30$g/kg is the factor of converting a unit of ice thickness to the mixed layer salinity increase along the sea ice growth process (Martinson & Iannuzzi, 1998). S_{z_c} represents the salinity at the z_c. z_c represents the critical depth above the UPL base, where entrainment is primarily driven by cooling, with negligible effects of salinization. In the present study, z_c is defined as 2 m above the aforementioned PD.

2.5. Sea Ice Growth Rate Estimate

The model SIC time series generally follows a sigmoid-like shape with an inflection point at around 50% (see Figures S2 and S3 in Supporting Information S1). The ice start day is defined as the first day on which $SIC > 0$. The slope of the sea ice growth rate (hereafter *IGR*, in % per day) is expressed as follows:

$$IGR = \frac{50}{\eta} \tag{5}$$

where η denotes the number of days between the ice start day and the day when SIC = 50% (see Figure S3 in Supporting Information S1). SIC time series were classified into three ice growth rate categories: (a) slow, (b) medium, and (c) fast growth (see Table S1 in Supporting Information S1). We find that slow ice growth cases are generally characterized by early initial ice formation, while fast ice growth cases have late ice formation (see Section 3.1). 200 SIC time series from the slow ice growth category are compared with 200 steepest SIC time series (with $IGR \geq 10.6$) from the fast sea ice growth group. These sets of SIC time series are presented, and the related physical processes are discussed. The selected 400 SIC time series were not determined by initial OHC (see Figure S4 in Supporting Information S1).

3. Results

3.1. Early Slow and Late-Fast Sea Ice Growth

The slow sea ice growth time series are generally associated with early sea ice formation; we refer to these as Early Slow. Similarly, the fast sea ice growth time series are associated with late ice formation, which we designate as Late-Fast (Figures 1a and 1b). The Early Slow sea ice growth cluster shows a spread of ice start day up to 20 days after 26 Sept., 2022 which is the date of the first initial ice formation (Figure 1a). In contrast, the Late-Fast sea ice growth cluster exhibits a spread of 6 days over 20–26 Oct., 2022, where 26 Oct. is the date of the last initial ice formation (Figure 1b). The model's early slowest sea ice growth is observed with an $IGR = 1.86\%.day^{-1}$ reaching 50% SIC at more than 3 weeks (27 days) after the ice start day (Figure 1a). The late-fastest sea ice growth has an $IGR = 13.91\%.day^{-1}$, reaching 50% SIC after only 4 days (Figure 1b). Note that the mean Early slow and Late-fast sea ice growth time series feature *IGR* of $1.79\%.day^{-1}$ and $8.33\%.day^{-1}$, respectively. The two distinct clusters suggest different thermohaline conditions or environmental processes influencing sea ice formation. The Early Slow cluster is more variable than the Late-Fast cluster. The difference in variability seems not to be originated from more variable atmospheric forcing in the early versus late fall, which we tested by forcing both sets of profiles by the same average atmospheric conditions. This resulted in no significant change in the two clusters' variability (see Figure S6 in Supporting Information S1). Further, no specific regional location influence is observed for the two clusters, meaning that the observed clusters are not confined to

specific regions (Figures 1c and 1d, and Figure S7 in Supporting Information S1). Additionally, the distance to the sea ice edge at the time of uCTD casts is not a good predictor of the initial ice formation timing (Figure 1d). This is surprising, since we expected that locations close to the sea ice edge would start to form ice earlier than those collected farther away. In the following section, we consider whether oceanic subsurface thermohaline conditions might be more determinant in the sea ice growth rate.

3.2. Thermohaline Profiles and Sea Ice Growth

In this section, haline and thermal stratification are analyzed with a focus on what causes Early Slow versus Late-Fast sea ice growth. Figures 2a–2h show T/S profiles along with N^2 profiles for both the early slowest (Figures 2a–2d) and the late-fastest (Figures 2e–2h) sea ice growth time series. From 6 days prior to ice start day to the day when SIC = 50%, the absolute salinity profiles of the early slowest sea ice growth exhibit a relatively strong salinity stratification with shallow large spikes of the N_S^2 in the UPL (Figures 2a and 2c). A transition of MLD from relatively shallow (<5 m) to nearly the pycnocline depth (∼15 m) is also observed (Figures 2a and 2b). In contrast, the thermohaline variation during the same time windows for the late-fastest sea ice growth exhibits a distinct homogeneous haline and thermal layer with MLD nearly in direct contact with the upper pycnocline depth (>20 m depth, Figures 2e–2h). Furthermore, the variation of the temperature profiles shows that the layers above the upper pycnocline depth for the early slowest sea ice growth is initially colder by −0.5°C relative to the late-fastest sea ice growth at ice start day (Figures 2b and 2f). However, the temperature profiles during the early slowest sea ice growth indicate a transition from a shallow thermocline to a point where the pycnocline and thermocline overlap at a depth of ∼15 m (Figure 2b). The pycnocline and the thermocline coincide in the case of the late-fastest sea ice growth case (Figure 2f), and the vertical temperature profiles are not associated with thermal gradient spikes (Figures 2d and 2h). One can notice that density stratification is dictated by the vertical salinity gradient, whereas the vertical temperature gradient is 10 times less in term of contribution to the vertical density gradient (Figures 2d and 2h).

The Early Slow salinity profiles are generally saltier by more than ∼0.5 g/kg relative to the Late-Fast profiles above 20 m depth prior to the initial sea ice formation and onward (Figure 2i). One can notice a weakening salt predominance in the Early Slow ice growth cluster (above 10 m depth after ice day, Figure 2i) inferring an increase in salt rejection processes driving rapid ice formation in the Late-Fast cluster, highlighting distinct brine dynamics between the two growth patterns. In addition, the Early Slow sea ice growth cluster exhibits a strong shallower (<3 m) stratified salinity layer (with N_S^2 up to 1.5 s^{-2}) than the Late-Fast cluster prior to the initial ice formation (Figure 2k). Furthermore, after the initial ice formation and onward, a deepening of persistent core of salinity stratified layer around the upper pycnocline is observed with the Early Slow sea ice growth cluster (Figure 2k).

The difference of temporal average of the time-depth temperature section between the Early Slow and Late-Fast sea ice growth clusters reveals that prior to the initial ice formation, the water column temperature of the Early Slow sea ice growth cluster is colder of about −1°C, and closer to the freezing point, than the Late-Fast sea ice growth cluster (Figure 2j). The salt stratified layer of the Early Slow sea ice growth cluster is associated with a warmer core pocket of temperature up to 1.5°C than the Late-Fast sea ice growth cluster prior to the initial ice formation and onward, and within 5-20 m depth (Figure 2j). In terms of thermal layering above the pycnocline, the Early Slow cluster exhibit a significant shallow temperature stratification which deepens along with the ice formation (Figure 2l). Note that the above findings are consistent with the model's output, when forced with the mean atmospheric conditions across the uCTD stations' area (see Figures S8 and S9 in Supporting Information S1).

3.3. Salt Deficit and Thermal Barrier Along Sea Ice Growth

As evidenced by the previous section with Figure 2, the water column of the Early Slow sea ice growth cluster experienced strong salinity stratification above the upper pycnocline depth. The thickness of the salinity stratified layer prior to the initial ice formation is about 75% of the top layer of the permanent pycnocline beneath the surface ML (Figure 3a). This stratified layer (UPL) decays slowly over more than 3 months (∼110 days) after the day of the initial ice formation, leading to the ML deepening to reach the upper pycnocline depth. In contrast, during the Late-Fast sea ice growth, the UPLT comprises only about 0−5% of the upper permanent pycnocline

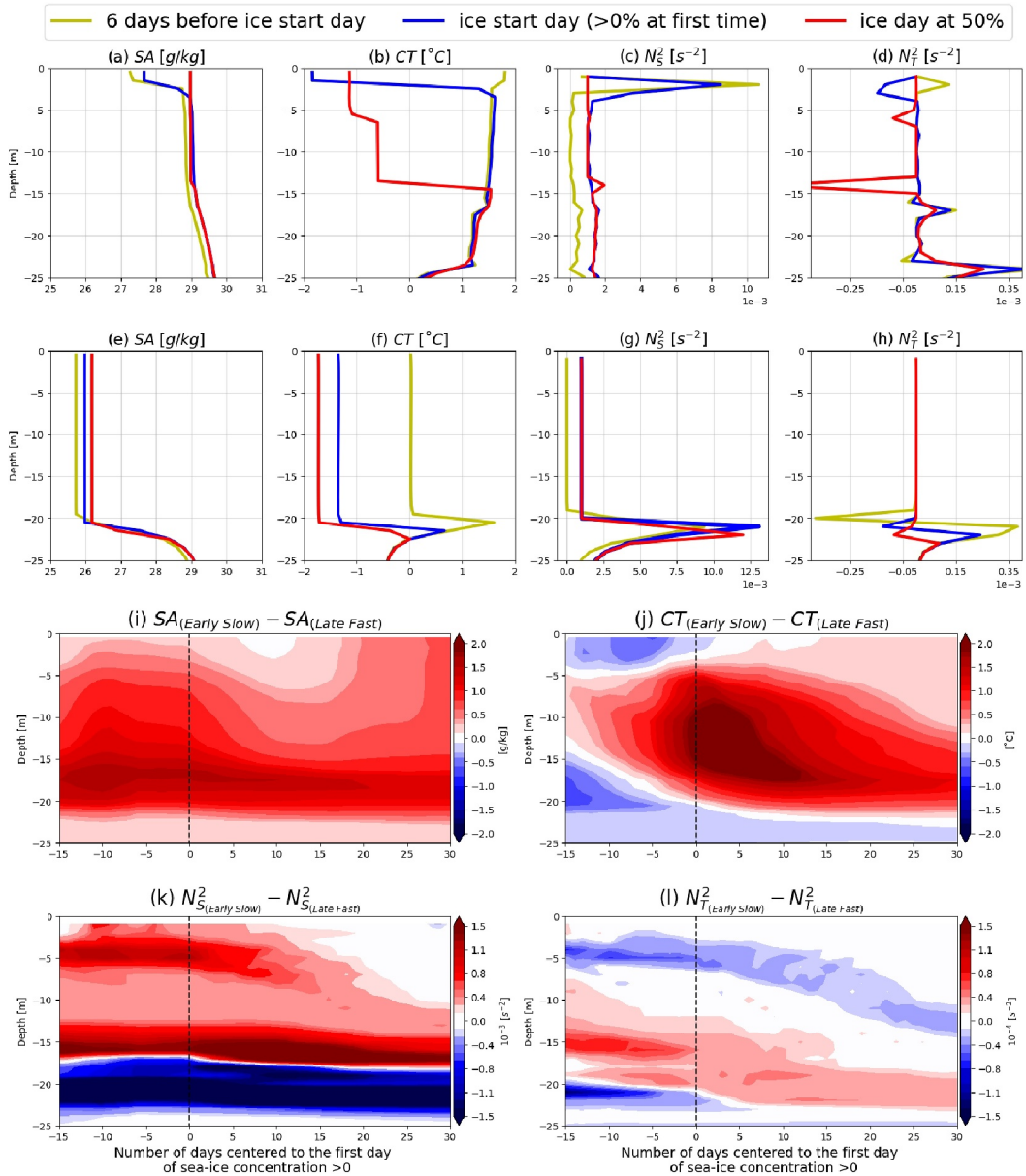

Figure 2. (a) SA, (b) CT, (c) $N_S^2$4, and (d) N_T^2 profiles are shown for three time points: 6 days before ice onset (yellow curve), on the ice day (blue curve), and on the day when SIC reaches 50% (red curve), based on the Early slowest sea ice growth time series from the model output. (e, f, j, h) Are same as (a, b, c, d) but based on the Late-fastest sea ice growth time series from the model output. Note that SA and N_S^2 are shifted respectively by 0.2 g/kg and $10^{-3}s^{-2}$ at ice start day (blue curve) and at day with SIC of 50% (red curve). (i) Represents the difference between the mean SA of Early slow sea ice growth and the mean SA of Late-fast sea ice growth. (j) Is the same as (i) but for the mean CT. (k, l) are the same as (i) but respectively for N_S^2 and N_T^2. Note: SA is the absolute salinity, CT is the conservative temperature, N_S^2 is the contribution salinity stratification to the vertical density gradient while N_T^2 is the contribution of temperature stratification to the vertical density gradient. The vertical black dashed line on (i, j, k, l) denotes the ice start day (zero on the *x*-axis).

before ice formation, keeping the mixed layer directly connected to the pycnocline and resulting in a nearly unstratified surface layer during rapid ice growth (Figure 3a).

The time series of salt deficit in the Early Slow case reveals significant salt rejection at rates above 20 cm per unit of ice prior to initial ice formation that drives surface mixed layer deepening and creates favorable conditions for freeze-up (Figure 3b). After ice formation, salt deficit remains high (about 25 cm per unit of ice) in this cluster. In

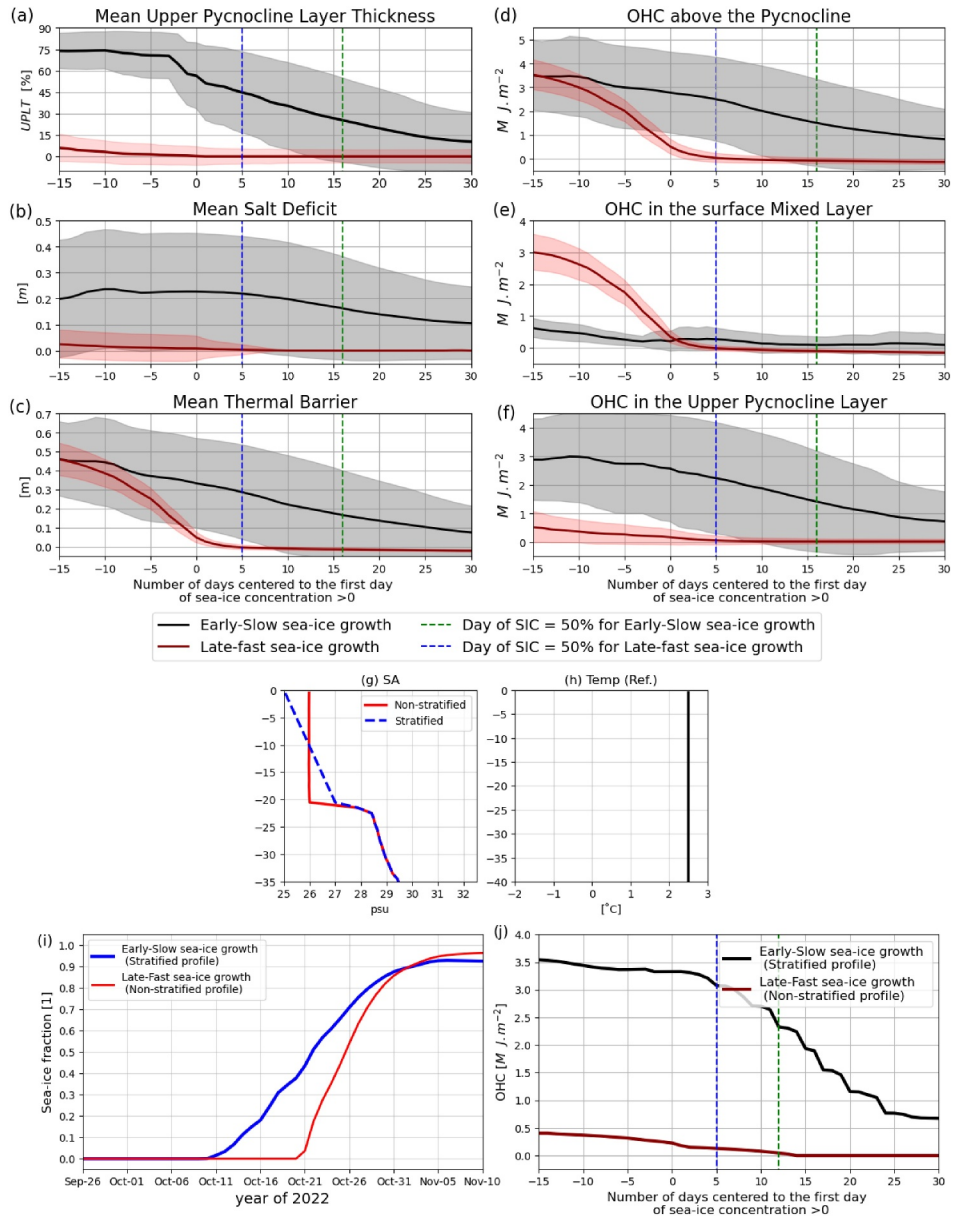

Figure 3. Time series of (a) the normalized mean upper pycnocline layer thickness, (b) the mean salt deficit (in m), (c) the mean thermal barrier (in *m*), (d) the mean OHC above the pycnocline (in M J.m^{-2}), (e) the mean OHC within the mixed layer (in M J.m^{-2}) and (f) the mean OHC within the upper pycnocline layer (in M J.m^{-2}). The vertical dashed black and green lines with doted horizontal barre indicate the day when the SIC reaches 50% respectively for the Early slow and Late-fast sea ice growth clusters. Thermohaline profiles for the idealized experiment: (g) non-stratified (red curve) and stratified (dashed blue curve) salinity profiles and (h) referred temperature profile (vertical black curve) to have identical initial heat content. (i) SIC time series for the non-stratified salinity profile (blue curve) and stratified salinity profile (red curve). (j) Same as in the (f). In this experiment (g–j), all simulations have started at the same date: Sept. 01, 2022.

contrast, the Late-Fast sea ice growth cluster exhibited weak salt deficit below 5 cm per unit of ice prior to initial ice formation. While the upper layers of both sea ice growth clusters are characterized by the same initial thermal barrier (up to ∼50 cm per unit of ice) beneath the ML, the thermal barrier decays faster, at ∼3cm/day per unit of ice, in the case of the Late-Fast ice growth cluster than in the Early Slow cluster (of ∼1 cm per unit of ice), which remains warm (Figure 3c). The persistent warm thermal barrier and shallow salinity stratification in the Early Slow cluster may explain its slower ice growth rate (Figures 2k, 2l and 3c).

3.4. Upper Pycnocline Heat Content Along Sea Ice Growth

To further elucidate the influence of the thermal barrier on the sea ice growth rate, the temporal variation of the ocean heat content (OHC) above the pycnocline is examined. The OHC of the surface layers is then divided into two main components: the OHC of the ML and the OHC of the UPL (Figures 3d–3f). The temporal variation of the OHC above the upper pycnocline exhibits nearly the same features as the Thermal Barrier along with both Early Slow and Late-Fast sea ice growth clusters (Figures 3c and 3d). Indeed, while characterized by the same OHC above the upper pycnocline 2 weeks prior to initial ice formation, the OHC in the case of the Late-Fast sea ice growth cluster decreases 6 times faster than in the Early Slow sea ice growth cluster ($\sim 2 * 10^5$ J.m^{-2} per day vs. $\sim 33 * 10^3$ J.m^{-2} per day, Figure 3d). One can notice that the observed upper salinity stratified layer of the Early Slow sea ice growth cluster has only lost ~ 0.5 MJ.m^{-2} by the ice start day, while the non-stratified upper layer of the Late-Fast sea ice growth cluster has lost up to ~ 3 MJ.m^{-2} (Figures 2k, 3a and 3d). After the sea ice day and onward, the OHC above the pycnocline of the Early Slow sea ice growth cluster remains high of $\sim 1-3$ MJ.m^{-2} and decays slowly about $66.7 * 10^3$ J.m^{-2} per day over a month (Figure 3d). About 86% of the observed heat loss above the pycnocline prior to initial ice formation occurred within the surface ML in the Late-Fast ice growth cluster, while about 86% occurred beneath the ML in the Early Slow ice growth case, which remains large onward (of $1-2.5$ MJ.m^{-2}, Figures 3e and 3f). That is, the salt stratified layer of the Early Slow sea ice growth is associated with large heat content and a thick thermal barrier. Thus, the remaining heat within the upper pycnocline layer of the Early Slow sea ice growth cluster is acting like a background heat source at the base of the surface mixed layer, delaying and preventing the complete freezing of the surface layer. The above results are consistent with the model's output, when forced with the mean atmospheric conditions across the uCTD stations' area (see Figures S8 and S10 in Supporting Information S1). In the next section, we demonstrate the role of salinity stratification on the timing of ice formation and its subsequent growth rate through an idealized experiment that focuses only on salinity stratification.

3.5. Role of Salinity Stratification in Sea Ice Growth

To further clarify the role of salinity stratification on the sea ice forming early and growing slowly, we performed an idealized experiment using two different salinity profiles: (a) non-stratified salinity profile (Figure 3g) and (b) stratified salinity profile with vertical gradient of ~ 0.1 g/kg.m above the pycnocline (Figure 3h). Both salinity profiles possess the same mean salinity of 26 g/kg above the pycnocline. All simulations use the same initial temperature profile (Figure 3i), ensuring each water column starts with identical heat content. The model is forced with the same average atmospheric forcing time series (see Figure S8 in Supporting Information S1). We find that the salinity stratified profile generates early ice formation followed by slow ice growth, while the non-stratified salinity profile forms ice later and faster (Figure 3j, similar to Figures 1a and 1b). Furthermore, with the stratified salinity profile, 74% of the OHC above the upper pycnocline is located beneath the mixed layer. This large portion of heat remains significant, decreasing at a rate of 10^5 J/m^2 per day for more than a month after ice formation begins (Figure 3k). Although each water column initially contains identical heat content in this experiment, in the case of non-stratified salinity, no heat remains beneath the mixed layer after ice formation begins. Furthermore, in the case of the stratified salinity profile, there is a remaining salt deficit of ~ 30 cm and thermal barrier ~ 30 cm per unit of ice after the ice day (see Figures S11 and S12 in Supporting Information S1). This demonstrates that, all else being equal, the upper ocean salinity stratification is determinant in the timing (early or late) and the rate (slow or fast) of sea ice growth.

4. Discussion and Conclusions

The present study uses a one-dimensional thermodynamic ocean-ice-column model (0-layer thermodynamic sea ice model, (Semtner, 1976)) from MITgcm to examine how salinity and temperature stratification above the pycnocline determine the timing and rate of sea ice formation in the Beaufort Sea. Forced by atmospheric conditions and initialized with uCTD data collected during the SASSIE campaign (fall 2022), the model ran 5 months (Sept 2022–Jan 2023) at each uCTD cast location in the Beaufort Sea. The model reproduces the observed mean SIC over the simulation time window very well: $r = 0.9$ and $RMSD = 0.07$. This agrees with Semtner (1976), who found that much of the seasonal variation in ice extent can be explained by thermodynamics alone. However, large fluctuations and interruption in the SIC time series driven by ocean-ice dynamics (Text S1 and Figure S1 in Supporting Information S1) are evidenced by observations while the model SIC time series are

typified by uninterrupted ice growth only. These differences between the model and observations are due to lateral interactions driven by advection processes, which are not included in the model. Advection, as a key process redistributing sea ice and heat, controls sea ice dynamics under atmospheric and oceanic forcing (Anheuser et al., 2023; Bi et al., 2019). Horizontal advection influences the thermohaline properties of the mixed layer (by shallowing and cooling), increases the rate of the freeze up, and promotes earlier ice formation (Crews et al., 2022).

Two ice formation regimes were identified from the model simulations: Early Slow and Late-Fast sea ice formation. We found that the water column of early sea ice formation is colder by 1°C with a shallow mixed layer and thicker upper stratified layer (up to 75% of the PD) than the later ice formation. The mixed layer in the earlier ice formation cluster starts at a temperature closer to the freezing point (approximately −1°C) and contains less heat content compared to the later ice formation cluster. Furthermore, before initial sea ice formation, the Early Slow sea ice growth cluster experiences strong salinity stratification and a large salt deficit (up to ∼25 cm per unit of ice) above the pycnocline. As a result, a colder and shallower surface mixed layer, reinforced by strong salinity stratification in the upper pycnocline, promotes earlier sea ice formation. In contrast, when the mixed layer is deep and the pycnocline aligns with the thermocline, heat content remains higher, and the required salt deficit is lower (<5 cm per unit of ice). This deeper mixed layer takes longer to ventilate, delaying sea ice formation.

During the 3 weeks following the ice day, we found that the Early Slow sea ice growth cluster remained strongly stratified and warm up to 1.5°C higher than the Late-Fast sea ice growth cluster. This warm core layer is primarily confined to the upper pycnocline, coinciding with the persistence of a thermal barrier even after the ice day. In contrast, the Late-Fast sea ice growth cluster quickly reaches the null heat content state. In addition, the UPLT of the Early Slow sea ice growth cluster is about 75% of the PD, meaning that significant downward convection driven destabilization is required for decaying the warm-salt stratified layer. The observed salinity stratified layer acts like a heat reservoir beneath the frozen surface mixed layer, leading to partial ice melt by convection during the sea ice growth period. Therefore, salinity stratification drives the upward heat flux rate, reducing the speed of sea ice growth, and might promote a delay in pack ice reconstruction. Even at high heat content, an upper layer typified by a deep ML with thermocline-pycnocline overlap promotes fast ice growth as a result of salinity stratification that isolates the surface from subsurface heat. This is consistent with Zhang et al. (2023), who reported that strengthened stratification limits mixing and heat flux, affecting sea ice thickness and timing. Accordingly, any heat lost from the surface consistently makes new ice. The idealized experiment conducted illustrates that, all else being equal, the upper ocean salinity stratification is determinant in the timing and the rate of sea ice growth. Thus, the one-dimensional thermodynamic sea ice growth rate is determined by the heat stored within the upper pycnocline layer which is defined by salinity stratification rather than the surface mixed layer heat content. Though changes in Arctic stratification from freshwater input and heat storage (Crews et al., 2022; Hordoir et al., 2022) alter sea ice retreat and advance, their full impact is uncertain.

Conflict of Interest

The authors declare no conflicts of interest relevant to this study.

Data Availability Statement

The underway CTD salinity and temperature data are available PO. DAAC via https://podaac.jpl.nasa.gov/dataset/SASSIE_L2_SHIPBOARD_UCTD_V1 (Schmidgall, 2023). All the model source codes are freely available, see Houndegnonto et al. (2025) (https://doi.org/10.5281/zenodo.16764198). The GMAO data sets of M2I1NXASM, M2T1NXFLX and M2T1NXRAD are available via https://disc.gsfc.nasa.gov/datasets/. The SIC data are collected from SAF (2017), while the ice motion data are collected from Tschudi et al. (2019).

Acknowledgments
The research described in this paper was carried out at the Jet Propulsion Laboratory (JPL), California Institute of Technology (Caltech), under a contract with NASA through the Salinity and Stratification at Sea Ice Edge (SASSIE) project (80NM0018D0004). The authors acknowledge Dr. Clement Bertin for the fruitful discussion throughout the present analysis. M. Steele was funded by the following Grants: NOAA NA20OAR4320271-AM212, ONR N00014-21-1-2868, NASA 80NSSC20K0768 and 80NSSC21K0832, and JPL subcontract 1709064.

References

Anheuser, J., Liu, Y., & Key, J. R. (2023). A climatology of thermodynamic vs. dynamic Arctic wintertime sea ice thickness effects during the CryoSat-2 era. *The Cryosphere*, *17*(7), 2871–2889. https://doi.org/10.5194/tc-17-2871-2023

Bi, H., Yang, Q., Liang, X., Zhang, L., Wang, Y., Liang, Y., & Huang, H. (2019). Contributions of advection and melting processes to the decline in sea ice in the Pacific sector of the Arctic Ocean. *The Cryosphere*, *13*(5), 1423–1439. https://doi.org/10.5194/tc-13-1423-2019

Cole, S. T., & Roemer, P. A. (2024). The transition layer and remnant transition layer of the Western Arctic Ocean: Stratification, vertical diffusivity, and Pacific summer water heat fluxes. *Journal of Geophysical Research: Oceans*, *129*(2), e2023JC020059. https://doi.org/10.1029/2023JC020059

Crews, L., Lee, C. M., Rainville, L., & Thomson, J. (2022). Direct observations of the role of lateral advection of sea ice meltwater in the onset of autumn freeze up. *Journal of Geophysical Research: Oceans*, *127*(2), e2021JC017775. https://doi.org/10.1029/2021JC017775

de Boyer Montégut, C., Madec, G., Fischer, A. S., Lazar, A., & Iudicone, D. (2004). Mixed layer depth over the global ocean: An examination of profile data and a profile-based climatology. *Journal of Geophysical Research*, *109*(C12). https://doi.org/10.1029/2004JC002378

Drushka, K., Westbrook, E., Bingham, F., Gaube, P., Dickinson, S., Fournier, S., et al. (2024). Salinity and Stratification at the Sea Ice Edge (SASSIE): An oceanographic field campaign in the Beaufort Sea. *Earth System Science Data Discussions, 2024*, 1–56. https://doi.org/10.5194/essd-2023-406

Francis, J. A., Vavrus, S. J., & Cohen, J. (2017). Amplified arctic warming and mid-latitude weather: New perspectives on emerging connections. *WIREs Climate Change*, *8*(5), e474. https://doi.org/10.1002/wcc.474

Gelaro, R., McCarty, W., Suárez, M. J., Todling, R., Molod, A., Takacs, L., et al. (2017). The Modern-Era Retrospective Analysis for Research and Applications, version 2 (MERRA-2). *Journal of Climate*, *30*(14), 5419–5454. https://doi.org/10.1175/JCLI-D-16-0758.1

GMAO. (2015a). Global Modeling and Assimilation Office (GMAO) (2015), MERRA-2 inst1_2d_asm_nx: 2d, 1-Hourly, instantaneous, single-level, assimilation, single-level diagnostics V5.12.4, Greenbelt, MD, USA, Goddard Earth Sciences Data and Information Services Center (GES DISC). https://doi.org/10.5067/3Z173KIE2TPD

GMAO. (2015b). Global Modeling and Assimilation Office (GMAO) (2015), MERRA-2 tavg1_2d_flx_nx: 2d, 1-Hourly, time-averaged, single-level, assimilation, surface flux diagnostics V5.12.4, Greenbelt, MD, USA, Goddard Earth sciences Data and Information Services Center (GES DISC). https://doi.org/10.5067/7MCPBJ41Y0K6

GMAO. (2015c). Global Modeling and Assimilation Office (GMAO) (2015), MERRA-2 tavg1_2d_rad_nx: 2d,1-hourly, time-averaged, single-level, assimilation, radiation diagnostics V5.12.4, Greenbelt, MD, USA, Goddard Earth Sciences Data and Information Services Center (GES DISC). https://doi.org/10.5067/Q9QMY5PBNV1T

Hibler, W. D. (1979). A dynamic thermodynamic sea ice model. *Journal of Physical Oceanography*, *9*(4), 815–846. https://doi.org/10.1175/1520-0485(1979)009⟨0815:ADTSIM⟩2.0.CO;2

Hordoir, R., Skagseth, y., Ingvaldsen, R. B., Sandø, A. B., Löptien, U., Dietze, H., et al. (2022). Changes in arctic stratification and mixed layer depth cycle: A modeling analysis. *Journal of Geophysical Research: Oceans*, *127*(1), e2021JC017270. https://doi.org/10.1029/2021JC017270

Houndegnonto, O. J., Fenty, I. G., Fournier, S., Steele, M., Zahn, J. M., & Gaube, P. (2025). 1d thermodynamic ocean ice column Mitgcm model for the study of thermohaline preconditioning for sea ice formation in the Beaufort Sea. *Zenodo*. https://doi.org/10.5281/zenodo.16764198

IOC, SCORIAPSO. (2010). IOC, SCOR and IAPSO, 2010: The international thermodynamic equation of seawater – 2010: Calculation and use of thermodynamic properties. (Tech. Rep.). Retrieved from https://www.teos-10.org/pubs/Getting_Started.pdf

Large, W. G., McWilliams, J. C., & Doney, S. C. (1994). Oceanic vertical mixing: A review and a model with a nonlocal boundary layer parameterization. *Reviews of Geophysics*, *32*(4), 363–403. https://doi.org/10.1029/94RG01872

Li, G., Cheng, L., Zhu, J., Trenberth, K. E., Mann, M. E., & Abraham, J. P. (2020). Increasing ocean stratification over the past half-century. *Nature Climate Change*, *10*(12), 1116–1123. https://doi.org/10.1038/s41558-020-00918-2

Martinson, D. G. (1990). Evolution of the Southern Ocean winter mixed layer and sea ice: Open ocean Deepwater formation and ventilation. *Journal of Geophysical Research*, *95*(C7), 11641–11654. https://doi.org/10.1029/JC095iC07p11641

Martinson, D. G., & Iannuzzi, R. A. (1998). Antarctic ocean-Ice interaction: Implications from ocean bulk property distributions in the Weddell gyre. In *Antarctic sea Ice: Physical processes, interactions and variability* (pp. 243–271). American Geophysical Union (AGU). https://doi.org/10.1029/AR074p0243

Miyawaki, O., Shaw, T. A., & Jansen, M. F. (2023). The emergence of a new wintertime Arctic energy balance regime. *Environmental Research: Climate*, *2*(3), 031003. https://doi.org/10.1088/2752-5295/aced63

Notz, D., & Community, S. (2020). Arctic sea ice in CMIP6. *Geophysical Research Letters*, *47*(10), e2019GL086749. https://doi.org/10.1029/2019GL086749

Rantanen, M., Karpechko, A. Y., Lipponen, A., Nordling, K., Hyvärinen, O., Ruosteenoja, K., et al. (2022). The Arctic has warmed nearly four times faster than the globe since 1979. *Communications Earth & Environment*, *3*(1), 1–10. https://doi.org/10.1038/s43247-022-00498-3

Ravindran, S., Pant, V., Mitra, A. K., & Kumar, A. (2021). Spatio-temporal variability of sea-ice and ocean parameters over the Arctic Ocean in response to a warming climate. *Polar Science*, *30*, 100721. https://doi.org/10.1016/j.polar.2021.100721

SAF, O. (2017). Global AMSR sea ice concentration—GCOM-W1, EUMETSAT SAF on Ocean and sea ice. https://doi.org/10.15770/EUM_SAF_OSI_NRT_2023

Schmidgall, C. (2023). *SASSIE Arctic field campaign shipboard uCTD data fall 2022 version 1| Physical oceanography distributed active archive center*. (PO.DAAC). Retrieved from https://podaac.jpl.nasa.gov/dataset/SASSIE_L2_SHIPBOARD_UCTD_V1

Schweiger, A. J., Steele, M., Zhang, J., Moore, G. W. K., & Laidre, K. L. (2021). Accelerated sea ice loss in the Wandel Sea points to a change in the Arctic's last ice area. *Communications Earth & Environment*, *2*(1), 1–11. https://doi.org/10.1038/s43247-021-00197-5

Semtner, A. J. (1976). A model for the thermodynamic growth of sea ice in numerical investigations of climate. *Journal of Physical Oceanography*, *6*(3), 379–389. https://doi.org/10.1175/1520-0485(1976)006⟨0379:AMFTTG⟩2.0.CO;2

Sérazin, G., Tréguier, A. M., & de Boyer Montégut, C. (2023). A seasonal climatology of the upper ocean pycnocline. *Frontiers in Marine Science*, *10*, 1120112. https://doi.org/10.3389/fmars.2023.1120112

Thomson, J., Smith, M., Drushka, K., & Lee, C. (2022). Air-ice-ocean interactions and the delay of autumn Freeze-Up in the Western Arctic Ocean. *Oceanography*, *35*(3–4), 76–87. https://doi.org/10.5670/oceanog.2022.124

Toole, J. M., Timmermans, M.-L., Perovich, D. K., Krishfield, R. A., Proshutinsky, A., & Richter-Menge, J. A. (2010). Influences of the ocean surface mixed layer and thermohaline stratification on arctic sea ice in the central Canada basin. *Journal of Geophysical Research*, *115*(C10). https://doi.org/10.1029/2009JC005660

Tschudi, M., Meier, W., Stewart, J., Fowler, C., & Maslanik, J. (2019). Polar pathfinder daily 25 km ease-grid sea ice motion vectors, version 4. *NASA National Snow and Ice Data Center Distributed Active Archive Center*. https://doi.org/10.5067/INAWUWO7QH7B

Wang, M., & Overland, J. E. (2015). Projected future duration of the sea-ice-free season in the Alaskan Arctic. *Progress in Oceanography*, *136*, 50–59. https://doi.org/10.1016/j.pocean.2015.01.001

Yamanouchi, T., & Takata, K. (2020). Rapid change of the arctic climate system and its global influences—Overview of Grene Arctic climate change research project (2011–2016). *Polar Science*, *25*, 100548. https://doi.org/10.1016/j.polar.2020.100548

Zhang, H., Bai, X., & Wang, K. (2023). Response of the arctic sea ice–ocean system to meltwater perturbations based on a one-dimensional model study. *Ocean Science*, *19*(6), 1649–1668. https://doi.org/10.5194/os-19-1649-2023

Zhong, W., Cole, S. T., Zhang, J., Lei, R., & Steele, M. (2022). Increasing winter ocean-to-ice heat flux in the Beaufort gyre region, Arctic Ocean over 2006–2018. *Geophysical Research Letters*, *49*(2), e2021GL096216. https://doi.org/10.1029/2021GL096216